

## Towards an integrated simulation of casting and structural performance of flowable fibre-reinforced concrete

Vidal Sarmiento, E.; Hendriks, Max; Geiker, M. R.; Kanstad, T.

**Publication date**

2016

**Document Version**

Accepted author manuscript

**Published in**

Proceedings of BEFIB 2016

**Citation (APA)**

Vidal Sarmiento, E., Hendriks, M., Geiker, M. R., & Kanstad, T. (2016). Towards an integrated simulation of casting and structural performance of flowable fibre-reinforced concrete. In *Proceedings of BEFIB 2016: 9th Rilem International Symposium on Fiber Reinforced Concrete, Sept 19-21, 2016, Vancouver, Canada* (pp. 1154-1168). RILEM publications.

**Important note**

To cite this publication, please use the final published version (if applicable). Please check the document version above.

**Copyright**

Other than for strictly personal use, it is not permitted to download, forward or distribute the text or part of it, without the consent of the author(s) and/or copyright holder(s), unless the work is under an open content license such as Creative Commons.

**Takedown policy**

Please contact us and provide details if you believe this document breaches copyrights. We will remove access to the work immediately and investigate your claim.

# TOWARDS AN INTEGRATED SIMULATION OF CASTING AND STRUCTURAL PERFORMANCE OF FLOWABLE FIBRE-REINFORCED CONCRETE

*Elena Vidal Sarmiento*<sup>1</sup>, *Max A.N. Hendriks*<sup>2</sup>, *Mette R. Geiker*<sup>3</sup>, *Terje Kanstad*<sup>4</sup>

<sup>1</sup> Postdoctoral fellow, Department of Structural Engineering, Norwegian University of Science and Technology (NTNU), Trondheim, Norway. elena.sarmiento@ntnu.no.

<sup>2</sup> Professor, Department of Structural Engineering, NTNU, Trondheim, Norway / Faculty of Civil Engineering and Geosciences, Department of Structural Engineering, Delft University of Technology, Delft, The Netherlands. M.A.N.Hendriks@tudelft.nl

<sup>3</sup> Professor, Department of Structural Engineering, NTNU, Trondheim, Norway. mette.geiker@ntnu.no.

<sup>4</sup> Professor, Department of Structural Engineering, NTNU, Trondheim, Norway. terje.kanstad@ntnu.no.

## ABSTRACT

Most recent studies on fibre-reinforced self-compacting concrete agree on the impact of the casting conditions on the fibre orientation and distribution, and its consequence thereof on the structural performance. A substantial number of investigations are continuously contributing to gain experience on the use of flowable FRC for different structural applications, and will ultimately serve to define the principles to incorporate the effects of fibre orientation and distribution on design recommendations.

The present paper describes a recent modelling approach that can take into account the configuration of the fibres in a structural element, i.e. their orientation and distribution, to predict the structural performance. The modelling approach has previously been presented and validated for structural elements in which the actual fibre configuration was characterized using Computer Tomography scanning. In this paper, the modelling approach is applied to analyse a wall element whose fibre configuration was obtained using the simulation of the concrete flow during casting.

The integrated simulation of casting and structural performance provides an actual framework to incorporate the effect of the fibre configuration in the prediction of structural behaviour. This should contribute to more reliable and effective use of fibre-reinforced self-compacting concrete.

*Keywords: Fibre reinforced self-compacting concrete, Fibre orientation, Fibre content distribution, Numerical simulation, casting, structural performance*

---

E.V. Sarmiento, Postdoctoral fellow  
Norwegian University of Science and Technology  
Richard Birkelands vei 1  
7491 Trondheim  
Norway

Email: elena.sarmiento@ntnu.no  
Tel: +47 73 59 50 72

## 1. INTRODUCTION

Like any other composite material, FRC needs to have low variation in the distribution of its components to be considered as a reliable material for engineering design (Chiachio, Chiachio, & Rus, 2012). Fibres need to provide consistent 3D reinforcement based on a homogeneous and random distribution. However, homogeneous flowable FRC is often difficult to achieve, because the inclusion of fibres creates an internal structure that counteracts the flow, affecting the desired compromise between fluidity and stability. This can hinder the uniform distribution of the fibres within structural elements and, furthermore, affect the mechanical behaviour. As Ferrara, Bamonte, Caverzan, Musa, and Sanal (2012) point out, areas with a reduced fibre dosage or no fibres act as flaws triggering early failures and activating unforeseen mechanisms that affect load-carrying capacity and structural performance.

Moreover, the orientation of fibres in a cast element often differs from the random orientation in a mixer. The material behaviour, the production and casting conditions, and the flow of concrete can influence the orientation of the fibres, and this strongly affects the mechanical properties of the cast element in the hardened state, see e.g. (Kooiman, 2000; Markovic, 2006; Soroushian & Lee, 1990; Stähli & van Mier, 2007). The loss of random orientation of the fibres may, in principle, jeopardize the use of the concrete because it makes the characterization and prediction of the structural behaviour more complex (Grünewald, Laranjeira, Walraven, Aguado de Cea, & Molins Borrell, 2012). However, a non-isotropic 3D structure in the fibre reinforcement could also be used to optimize the performance of the material, for instance, by tailoring the predominant fibre orientation to meet the principal tensile stress direction. Several authors (Ferrara et al. 2011; Martinie and Roussel 2011) have stated the basic principles for a tailored orientation of fibres: controlling the casting conditions and ensuring appropriate rheological properties. The effective orientation of the fibres may improve the mechanical behaviour of the FRC (Barnett, Lataste, Parry, Millard, & Soutsos, 2010; Boulekbache, Hamrat, Chemrouk, & Amziane, 2010; Ferrara, Ozyurt, & di Prisco, 2011) and lead to the more efficient design of a structural element.

In Elena Vidal Sarmiento (2015) a novel modelling approach was presented in which the fibre structure was taken into account in simulating the mechanical behaviour of FRC elements. The actual fibre structure was experimentally determined using CT scanning. This made it possible to validate the predicting ability of the proposed approach. In practice, though, CT scans will not be available. In this paper, the approach is applied to a structural element whose fibre structure is obtained using simulation of the concrete flow during casting. The aim is to demonstrate the coupling between the two simulation approaches.

The demonstration example comprises the analysis of a wall element cast with self-compacting FRC. The investigation by Døssland (2008) revealed large variation in fibre orientation within wall elements using a vertical casting process. This study served as a precedent for later analysis of these elements at the Norwegian University of Science and Technology. The wall element here presented was described in Žirgulis, Švec, Geiker, Cwirzen, and Kanstad (2016). The authors performed numerical simulations of the casting process and a comparison of the fibre orientation with experimental results. Standard test elements were sawn from the wall element. For this reason, full-scale testing was not possible and experimental results are not available to validate the results of the present study.

The first part of this paper introduces the modelling approach developed to include the fibre structure when simulating the mechanical behaviour of structural elements cast with flowable FRC. In the second part, the fibre structure from the simulations of the vertical wall casting presented in Žirgulis et al. (2016) is incorporated in the numerical approach to investigate the flexural behaviour of the wall element in relation to the inhomogeneity of the fibre orientation and distribution.

## 2. DESCRIPTION OF THE MODELLING APPROACH

This section describes the modelling approach presented in Elena Vidal Sarmiento (2015) for analysing FRC structural elements. Since the material cannot be assumed to be homogeneous on the

scale of the structural element, a spatial discretization of the element is defined within which the material can be considered homogeneous, thus assuming volume-wise constant material properties. The process consists of: obtaining the fibre structure (Figure 1a), discretizing the structural element in volumes (Figure 1b), determining the fibre structure properties within each discrete volume (Figure 1c), defining an adequate constitutive model that describes the behaviour of the FRC at the discrete volume level making use of the fibre structure properties, and finally, simulating the structural response using finite element (FE) modelling (Figure 1d).

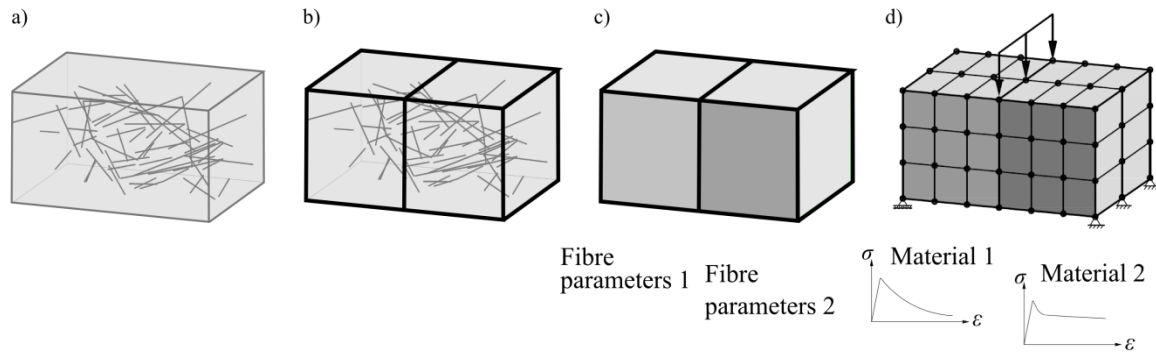


**Figure 1.** a) Matrix and fibre structure, b) discretization in volumes, c) characterization of the fibre parameters, and d) finite element model.

The constitutive model is applied at an intermediate level which is between the fibre level and the structural element level. It uses a single-phase material definition, with the consequent computational advantages for application to structural elements. In this way, the definition of the matrix-fibre interface behaviour is circumvented. However, a new issue is raised. In the absence of well-established constitutive modelling technique for this intermediate level, heuristic assumptions were used for the constitutive modelling.

### 2.1. Fibre parameters within a discrete volume

The modelling approach requires a complete characterization of the fibre structure, that is the precise position of every fibre. Several methodologies can be utilized for assessing the fibre structure of an FRC element, including flow simulations (Švec, Skoček, Stang, Olesen, & Poulsen, 2011), numerical algorithms based on probabilistic distributions (Cunha, Barros, & Sena-Cruz, 2012), X-ray Computed Tomography (CT) (Stähli, Custer, & van Mier, 2008), and visualization of fibres within a viscous transparent fluid (Zhou & Uchida, 2013).

To define the local fibre properties, a discretization of the structural element in volumes is considered. The discrete volume size should take into account criteria related to the size of the fibres and be sufficiently descriptive of the inhomogeneities of the fibre structure. Fibre properties are determined considering the fibres located in each volume. Because fibres can intersect one or several discrete volumes, the intersection points with the boundaries of the volumes need to be determined. In this way, each segment of a fibre is considered in the volume in which it is located (Figure 1b). Intersection points are obtained by assuming that fibres are perfectly straight.

This model incorporates the information from the spatial distribution of the fibres which can potentially influence the mechanical performance of a flowable FRC element, namely the fibre orientation and the local fibre content. The fibre orientation pattern of a body can be described using a set of second-order orientation tensors (Advani & Tucker, 1987; Ferrara et al., 2011; Şanal & Özyurt Zihnioğlu, 2013; Švec, Žirgulis, Bolander, & Stang, 2014) defined over a set of discrete volumes of the body. Each orientation tensor describes the fibre orientation state within the volume and can be defined as:

$$\mathbf{A} = \frac{\sum_n L_n \mathbf{p}_n \mathbf{p}_n^T}{\sum_n L_n} \quad (1)$$

where  $\mathbf{A}$  is the orientation tensor of a discrete volume. For all the fibres and fibre segments in the volume,  $\mathbf{p}_n$  is a unit vector in the fibre direction, and  $L_n$  is the length of the fibre or fibre segment. The dominant fibre direction ( $\mathbf{a}_1$ ) can be obtained as the eigenvector associated with the largest eigenvalue of the orientation tensor.

The second aspect, the local fibre content, is expressed in terms of volume fraction ( $v_f$ ) and can be computed for each discrete volume as:

$$v_f = \frac{\sum_n L_n A_f}{V_c} \quad (2)$$

where  $A_f$  is the fibre cross-section area and  $V_c$  the discrete volume. The procedure described here makes it possible to represent the orientation and distribution pattern of a structural element by choosing a certain discretization of the element in volumes and assessing the fibre parameters  $\mathbf{a}_1$  and  $v_f$  within each discrete volume. This is illustrated in Figure 2 for the example shown in Figure 1a.

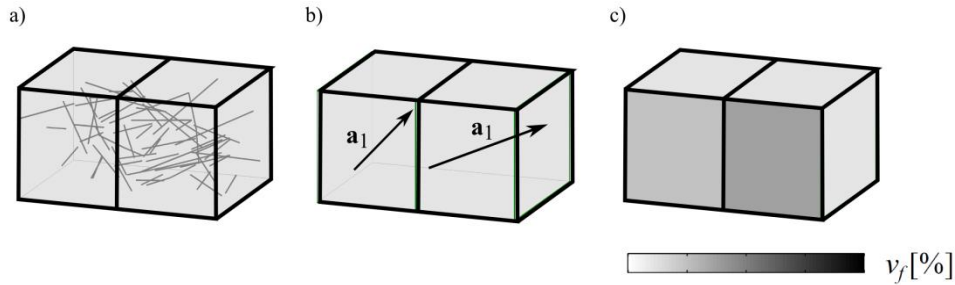


**Figure 2.** a) Orientation ellipsoids and dominant fibre orientation, and b) fibre volume fraction.

## 2.2. Definition of fibre efficiency

When a crack arises, the efficiency of a fibre that bridges the crack depends on its orientation with respect to the crack plane. This can be expressed by the angle  $\theta$  between the direction normal to the crack plane ( $\mathbf{n}$ ) and the fibre direction. In a similar manner, it can be assumed that the efficiency of a group of fibres depends on the angle between  $\mathbf{n}$  and the dominant fibre direction of the group of fibres  $\mathbf{a}_1$ . This can be considered a valid assumption whenever there is a certain degree of unidirectionality. For the group of fibres in each discrete volume, the angle with respect to the crack plane may therefore be formulated as:

$$\cos\theta = \mathbf{a}_1 \cdot \mathbf{n} \quad (||\mathbf{a}_1|| = ||\mathbf{n}|| = 1) \quad (3)$$

Figure 3 depicts two fibre orientation states represented by the dominant directions  $\mathbf{a}_1$  and illustrates the relevance of the variable  $\cos\theta$  as a measure of fibre efficiency.

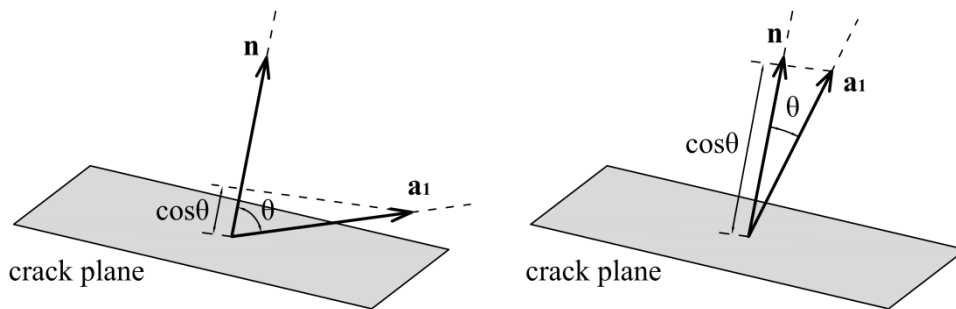


**Figure 3.** Orientation state of fibres represented by  $\mathbf{a}_1$  for a) a predominantly unfavourable orientation, and b) a favourable orientation.

For convenience, a single variable is introduced that integrates the local fibre orientation with the local volume fraction. This fibre efficiency variable  $\mu$  is defined as a linear combination:

$$\mu = w_1(\cos\theta) + w_2\left(\frac{v_f}{\bar{v}_f}\right) \quad (4)$$

where  $w_1$  and  $w_2$  are weightings for the orientation and volume fraction components, respectively (with  $w_1 + w_2 = 1$ ), and  $\bar{v}_f$  is the nominal fibre volume fraction of the mix.

It is worth noting that  $\mathbf{a}_1$  and  $v_f$  are material parameters that describe the characteristics of the fibres in each discrete volume of the specimen. In contrast,  $\cos\theta$  and therefore also  $\mu$  are evaluated at each integration point of the FE model, and they are actually variables that depend on the cracking model adopted and the crack plane, so they may change during the simulation. It is worth noting that the FE mesh may not necessarily coincide with the discretization of the fibre structure (as depicted in Figure 1d).

### 2.3. Constitutive modelling

Because the main contribution of fibres occurs after the crack initiation, both compressive and pre-cracking response can be assumed to agree with those of plain concrete. The local fibre properties are thus incorporated to define the post-cracking tensile behaviour. The uniaxial stress-strain relationship depicted in Figure 4 is proposed to describe the  $\sigma$ - $\varepsilon$  behaviour in tension. This diagram describes an initial linear-elastic response up to the tensile strength ( $\sigma_1$ ), which characterizes the onset of cracking.

The residual tensile strength  $\sigma_2$ , which defines an ideal plastic post-cracking behaviour, is defined dependant on the fibre efficiency parameter  $\mu$ . When the local value of  $\sigma_2$  results in strain softening, the post-peak drop is assumed to follow the behaviour of plain concrete, until the intersection with the residual post-cracking branch (point (2) in Figure 4a). On the contrary, when  $\sigma_2$  exceeds the tensile strength  $\sigma_1$ , leading to a hardening response, the residual strength is assumed to be reached at a strain corresponding to a crack opening of 0.5 mm. Only the strain level  $\varepsilon_2'$ , which is associated with localization of the crack, is regularized in terms of the finite element size. It should be noted that the focus of this paper is on the use of a material model based on actual fibre structure, rather than proposing a more sophisticated description of the stress-strain behaviour for the numerical implementation.

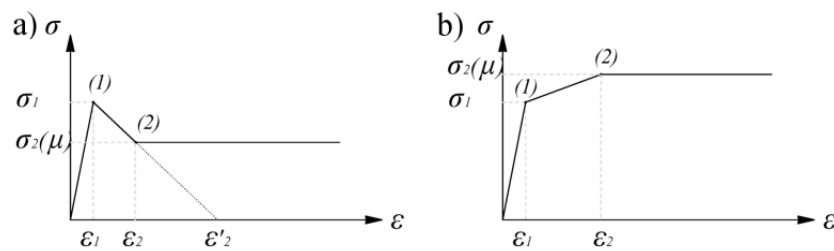


**Figure 4.** Uniaxial tensile stress-strain relationship for a) strain softening, and b) strain hardening behaviour.

The relationship between the residual tensile strength  $\sigma_2$  and the fibre parameter  $\mu$  needs to be established for the particular material, type and geometry of fibres, as well as for the concrete properties where fibres are embedded in.

The uniaxial stress-strain behaviour in Figure 4 can be generalized to multiaxial stress and strain states by embedding it in a rotating crack model based on a total strain concept, see e.g. Rots (1988). This means that an explicit modelling of the shear retention after cracking is not needed. During an analysis, upon rotation of the principal strains, the (potential) crack orientation rotates and the uniaxial stress-strain behaviour normal to the crack changes too, since it depends on the angle  $\theta$  with the dominant fibre direction.

The dependence of the uniaxial stress-strain relationship on the fibre parameters and on the crack direction is shown in Figure 5. This figure illustrates an FRC specimen similar to that in Figure 1a-c. For the sake of clarity, the FE mesh coincides with the volume discretization of the fibre structure in this case. The uniaxial tensile stress-strain relationship at the integration point of each element depends on two main aspects: 1)  $\mathbf{a}_1$  and  $v_f$  as the fibre parameters, and 2) the direction normal to the crack ( $\mathbf{n}$ ), which depends on the current state of stresses. In Figure 5a, the stress-strain relationships of the two elements differ depending on the dominant fibre direction of each element. Similarly, in Figure 5b the stress-strain relationships differ based on a variation in the fibre content. Unlike the two previous cases, the two elements in Figure 5c have the same fibre parameters, but this time different crack directions. Depending on  $\mathbf{n}$ , the variable  $\mu$  and therefore also  $\sigma_2$  are different in each element, which leads once again to two different stress-strain relationships.

This modelling approach is therefore able to take into account both the inhomogeneities of the fibre structure and the dependence of the material on the direction of the principal strains, which is related to the anisotropic behaviour of the material.

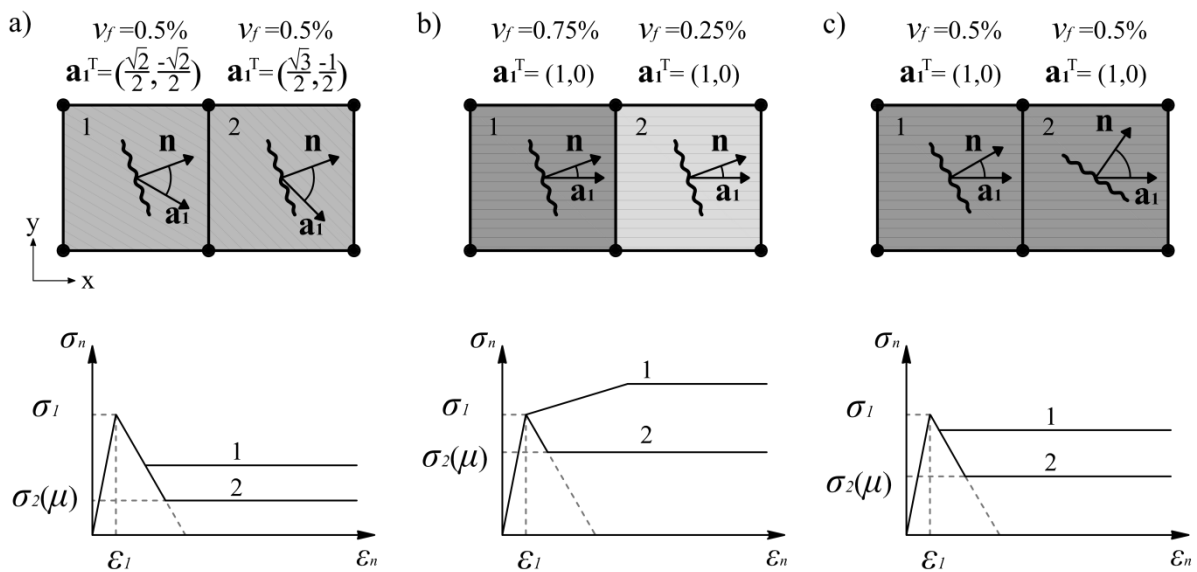


**Figure 5.** Tensile constitutive model for two elements with differences in a) fibre orientation, b) fibre volume fraction, and c) the direction normal to the crack.

### 3. SIMULATION OF VERTICAL WALL CASTING

A numerical framework was recently developed by Švec et al. (Švec & Skoček, 2013; Švec, Skoček, Stang, Geiker, & Roussel, 2012) which is capable of predicting the free surface flow of a suspension of rigid particles in a non-Newtonian fluid. The framework is a combination of the lattice-Boltzmann method for fluid flow, a mass tracking algorithm for free surface representation, the immersed boundary method for two-way coupled interactions between fluid and rigid particles, and an algorithm for the dynamics and mutual interactions of rigid particles. The numerical framework models steel fibres as thin rigid cylinders and takes into account features such as the interaction between the fluid and the fibres, collisions between the fibres or between the fibres and the formwork, though unfortunately it does not include the segregation effect.

This numerical framework was used to simulate the vertical casting process of the wall element illustrated in Figure 6. This wall element was cast using self-compacting FRC containing 0.5% vol. of steel fibres, which had hooked-ends, a length of 60 mm, an aspect ratio of 80. The casting point was located close to one edge of the wall. Four tie bars were used to tie the vertical walls of the formwork, see Figure 6. In addition to the wall element, nine standard beams (150 mm  $\times$  150 mm  $\times$  550 mm) were cast for three-point bending testing in accordance with EN14651 (European Standard, 2005).

The mix design, mixing procedure, fresh concrete properties and casting process are described in detail in Žirgulis et al. (2016).

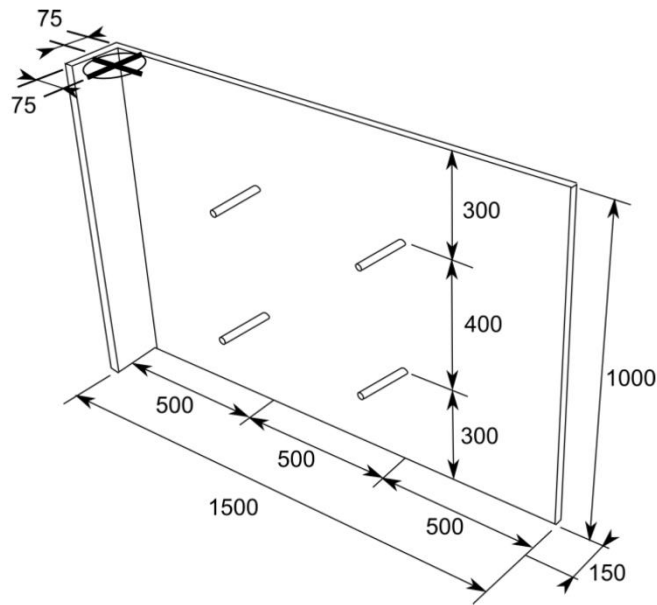


**Figure 6.** Formwork dimensions, casting point, and position of the four tie bars. Dimensions in mm (Žirgulis et al., 2016).

At the end of casting, fibre orientation appeared to be strongly influenced by the casting process. Most of the fibres were horizontally oriented in the area below the casting point and close to the bottom surface of the formwork. Furthermore, the results revealed a great impact of the tie bars on the fibre orientation and distribution. In Žirgulis et al. (2016), the simulated fibre orientation pattern was compared to the actual fibre structure, which was experimentally investigated using CT scanning. The comparison showed reasonably good agreement and validated the use of the numerical simulation tool.

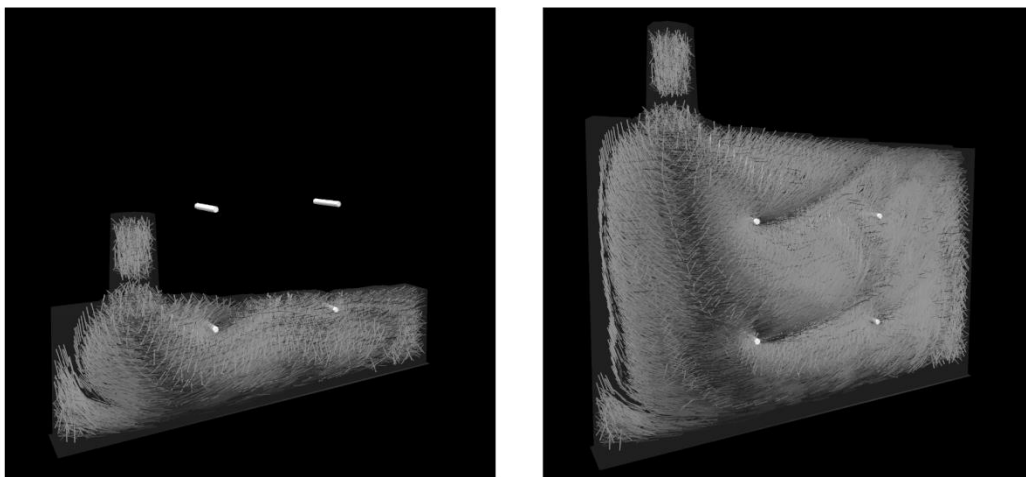


**Figure 7.** Simulation of fibre orientation during vertical wall casting<sup>1</sup>. The white bars represent the bars used to tie the vertical walls of the formwork.

<sup>1</sup> [www.dti.dk/4c-flow/33808](http://www.dti.dk/4c-flow/33808)

## **4. SIMULATION OF STRUCTURAL RESPONSE OF A WALL ELEMENT**

The modelling approach described in Section 2 is applied to predict the mechanical behaviour of the wall element based on the fibre structure obtained with the simulation of the casting process. The impact of the fibre orientation and distribution on the structural behaviour is discussed based on a comparison with a model that assumes homogenous and isotropic material properties.

### **4.1. FRC as an inhomogeneous and anisotropic material**

The flow simulation presented in Section 3 can fully describe the fibre structure in the investigated wall by providing the location of every fibre at the end of casting. The fibre structure was discretized in volumes with dimensions of 50 mm × 50 mm × 150 mm, in length, height and thickness direction, in order to define the local fibre properties. The variations of the fibre orientation and distribution across the element thickness were negligible, which explains why the wall was not discretised in that direction.

The fibre skeletons in Figure 8a provides a first insight into the inhomogeneous and anisotropic fibre structure. The figure illustrates the skeleton of fibres in a longitudinal slice just 50 mm thick to avoid a too dense image. Figure 8b and c illustrate the set of local volume fractions and dominant fibre directions obtained from the fibre structure. The grayscale map reveals an uneven fibre distribution within the wall, though the low fibre content along the edges seems unrealistic.

The nonlinear FE simulation of the wall was addressed as a 2D plane stress problem. Eight-node quadrilateral plane stress elements with  $2 \times 2$  Gauss integration were used. The model was defined with the element size (50 mm × 50 mm × thickness of the wall) coinciding with the volume discretization of the fibre structure. The model is denoted 50/50, where the first term refers to the volume discretization and the second term indicates the size of the finite elements.

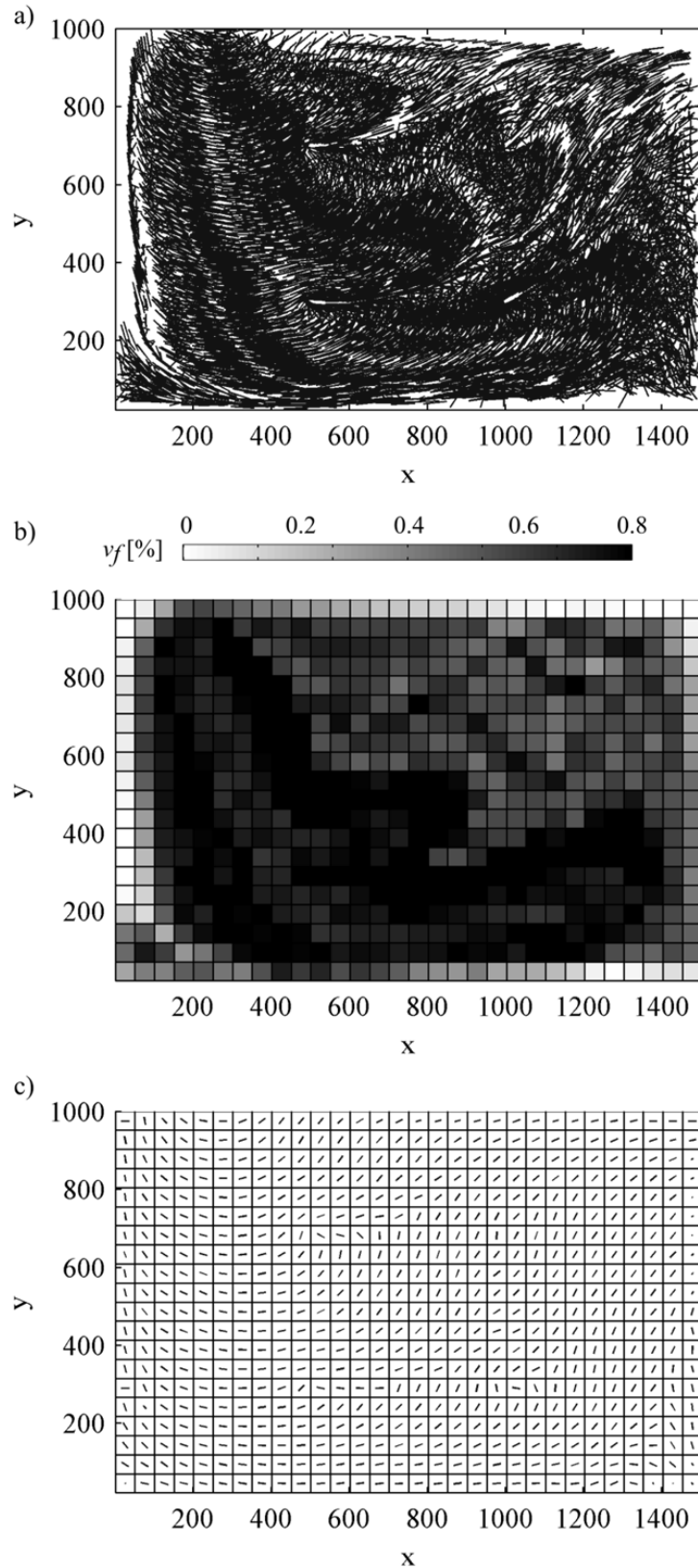


**Figure 8.** a) Skeleton of fibres, b) local volume fractions and c) dominant fibre directions ( $\mathbf{a}_1$ ).

An imaginary loading was applied at the central point at the topside of the wall. The horizontal displacement of this point was constrained, as well as the vertical displacement of the two supports (Figure 9). The load was applied incrementally using displacement control. A linear elastic behaviour

was assumed for the elements adjacent to the supports and loading point. The convergence criterion was set at 5% based on a force norm.

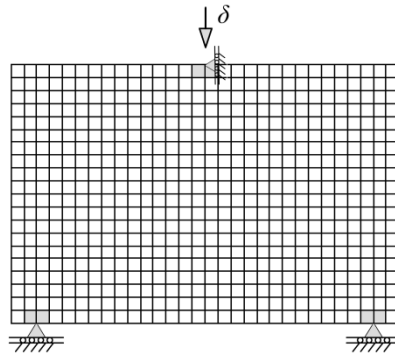


**Figure 9.** Mesh with 50 mm × 50 mm elements, supports and loading system for a wall element.

The nonlinear behaviour of the material was modelled with a rotating smeared crack model based on a total strain concept. The compressive behaviour was defined using an elastic-ideal plastic stress-strain model. The uniaxial tensile stress-strain model was assumed to be as depicted in Figure 4. Most parameters were derived from experimental data and are related with the composition and characteristics of the FRC under consideration. The calibration of the material parameters was already described in E. V. Sarmiento, Hendriks, and Kanstad (2014). Table 1 summarizes the material parameters considered in this case study.

**Table 1.** Material input parameters.

Material parameter	
Young modulus [MPa]	38000
Compressive strength [MPa]	65
Fracture energy of plain concrete, $G_F$ [N/mm]	0.154
Tensile strength, $\sigma_t$ [MPa]	3.8
$\varepsilon_1$ [-]	$1.0 \cdot 10^{-4}$
$\varepsilon_2'$ [-]	$8.6 \cdot 10^{-4}$
$\varepsilon_2$ [-]	$1.6 \cdot 10^{-3}$

The FE modelling evaluates the fibre efficiency variable  $\mu$  at each integration point based on the fibre parameter  $v_f$  and the angle  $\theta$  between the fibre dominant orientation ( $\mathbf{a}_1$ ) and the principal strain direction (see Eq. (4)). The model thus assesses the residual tensile strength  $\sigma_2$  that defines completely the uniaxial stress-strain model. Eq. (5) and (6) describe the relationship between  $\sigma_2$  and  $\mu$ . For the present mix, this relationship was established in E. V. Sarmiento et al. (2014) from the analysis of an experimental set of 15 specimens which covered a wide range of fibre dispersions.

$$\sigma_2 = 7.20 \mu - 3.20, \quad \text{if } \mu \geq 0.5 \quad (5)$$

$$\sigma_2 = 0.77 \mu, \quad \text{if } \mu < 0.5 \quad (6)$$

This model is therefore able to take into account the inhomogeneities of the fibre structure and the anisotropic behaviour of the material.

## 4.2. FRC as a homogeneous and isotropic material (Reference model)

A reference model, denoted Reference/50, was considered for the purpose of comparison. This model did not incorporate the local fibre parameters. The material behaviour was therefore assumed to be isotropic and homogeneous throughout the wall element. The uniaxial tensile behaviour was defined in accordance with Figure 4, but in this case the residual tensile strength  $\sigma_2$  was fixed as any other parameter of the diagram. Its value was derived from three-point bending tests of the standard beams cast in addition to the wall, and calibrated in accordance with the relationship  $\sigma_2 = f_{R3}/3$  (fib, 2010). The average residual flexural tensile strength  $f_{R3}$  obtained for the nine beams was 8.9 MPa; therefore  $\sigma_2$  was assumed to be 3.0 MPa.

The material parameters and the FE mesh for this model were the same as those for the 50/50 model (Table 1, Figure 9).

## 4.3. Analysis results

Figure 10 compares the load-displacement curves of the 50/50 and Reference/50 models. As expected, the two models predict exactly the same load-deflection relationship up to the onset of cracking. Figure 12-Figure 15 illustrate the crack propagation phenomenon of the two models using contour plots that depict the maximum principal strain at the deflection stages A-D indicated in Figure 10. The strain levels considered in the contour plots are defined in Figure 11.

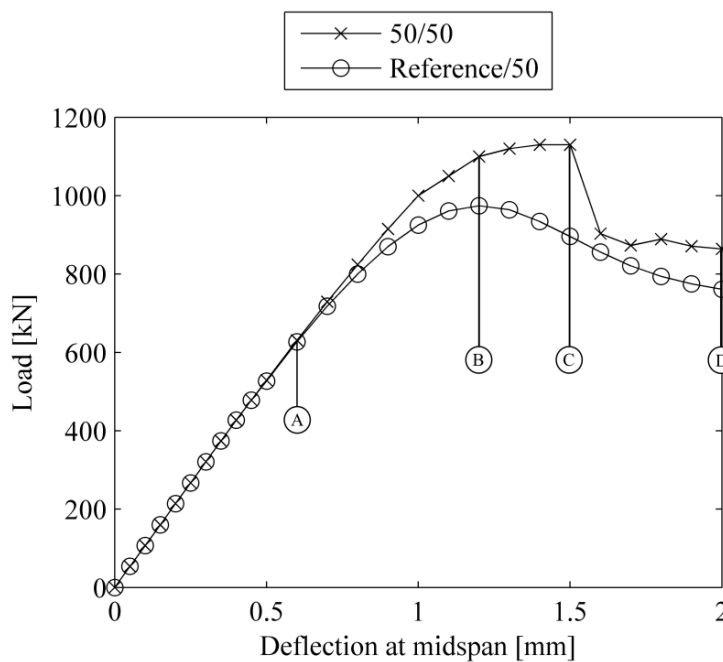


**Figure 10.** Load-deflection responses of the wall for 50/50 model, and Reference/50 model.

At stage A, cracking has been initiated in the lower part of both models (Figure 12). The Reference/50 model reaches the peak load at the deflection level B. At this stage the damage zone has extended and large strains concentrate at midspan in the lower part of the wall (Figure 13a). From that point on, the damage area grows upwards (Figure 13a-Figure 15a), and the load decreases gradually; at stage D the value is 79% of the peak load.

At stage B, the 50/50 model sustains 13% larger load than the Reference/50 model. Moreover, Figure 13b shows a smaller area of large strains compared to Figure 13a. The load increases up to stage C, at which the value is 26% larger than for the Reference/50 model. Increasing the deflection causes a sudden load reduction. At stage D, the applied load is 76% of the peak load. For the 50/50 model,

damage extends over a larger area than for the Reference/50 model, and large strains do not propagate uniformly, but are governed by the local material properties (Figure 14b-Figure 15b).

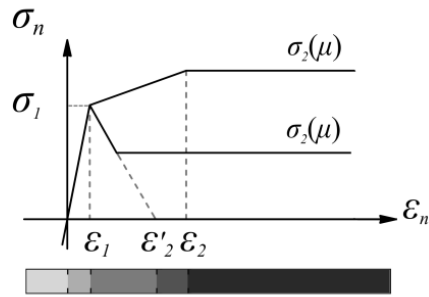


**Figure 11.** Strain levels defined over the uniaxial tensile stress-strain relationship for Figure 12-Figure 15.

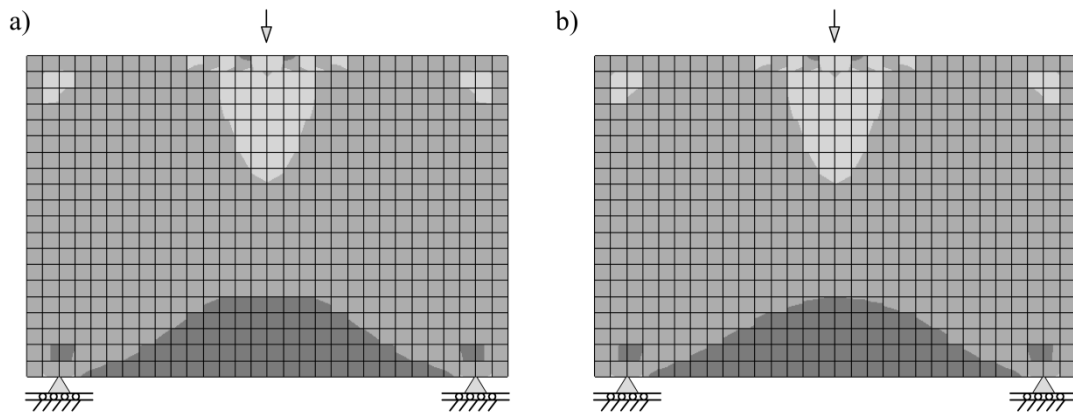


**Figure 12.** Strain levels of the maximum principal strain of the wall at a deflection level A (Figure 10) for: a) Reference/50 model, and b) 50/50 model (grayscale levels are defined in Figure 11).

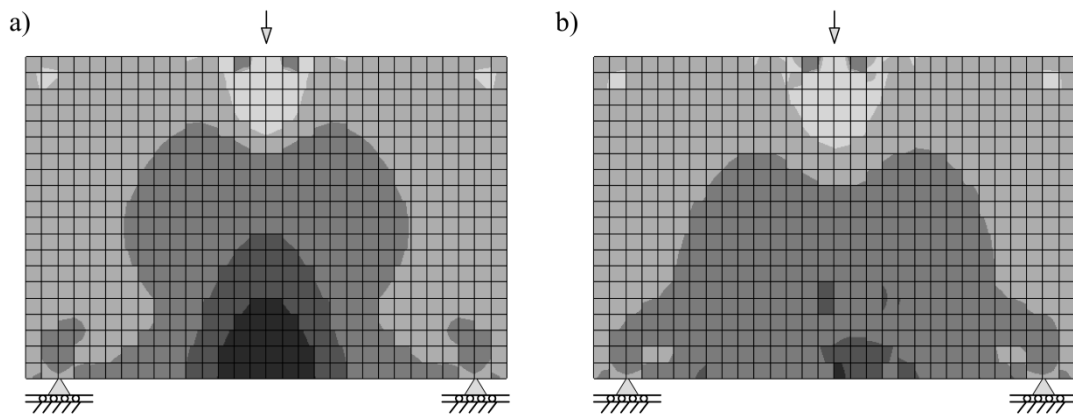


**Figure 13.** Strain levels of the maximum principal strain of the wall at a deflection level B (Figure 10) for: a) Reference/50 model, and b) 50/50 model (grayscale levels are defined in Figure 11).

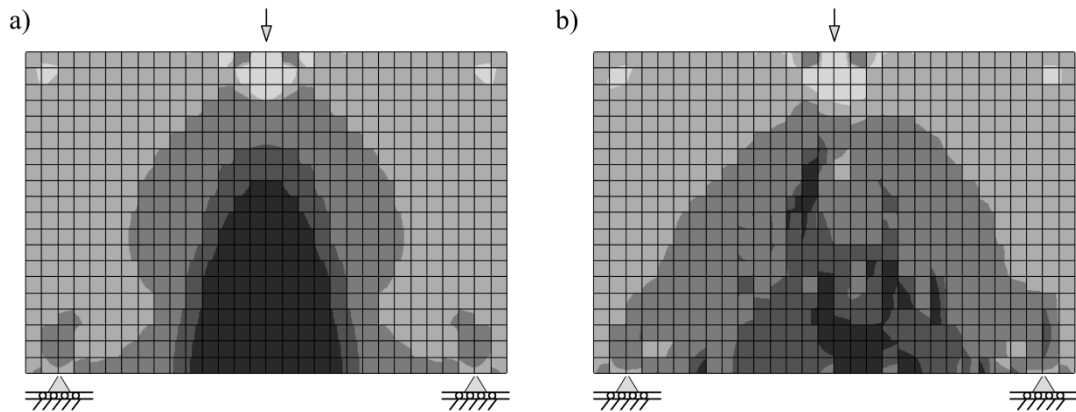


**Figure 14.** Strain levels of the maximum principal strain of the wall at a deflection level C (Figure 10) for: a) Reference/50 model, and b) 50/50 model (grayscale levels are defined in Figure 11).

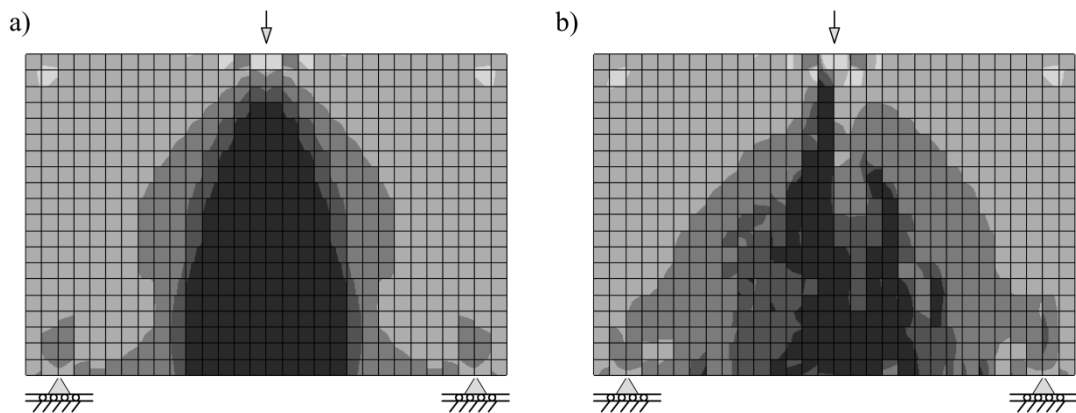


**Figure 15.** Strain levels of the maximum principal strain of the wall at a deflection level D (Figure 10) for: a) Reference/50 model, and b) 50/50 model (grayscale levels are defined in Figure 11).

The results in Figure 10 indicate that modelling the walls disregarding the inhomogeneous and anisotropic fibre configuration leads, in this case, to an underestimation of the load-carrying capacity.

## 5. CONCLUSIONS

In this paper, the coupling between the simulation of the casting process and the modelling approach presented in Elena Vidal Sarmiento (2015) was demonstrated. For such purpose, the flexural behaviour of a wall element cast with self-compacting FRC was analysed. The fibre structure simulated in Žirgulis et al. (2016) was incorporated in a FE model based on the principles of the proposed modelling approach. The analysis was able to take into account the inhomogeneities of the fibre structure and the anisotropic behaviour of the material. This model was compared with a reference model, in which the behaviour of the FRC was assumed to be isotropic and homogeneous throughout the wall element. The comparison of the results revealed significant differences in the load-carrying capacity and in the crack pattern. Furthermore, the results suggest that for this particular case, the uneven fibre distribution and orientation resulting from the casting process could lead to a favourable impact on the load-carrying capacity in comparison with an isotropic configuration of the fibres.

The coupling between simulation tools offers a comprehensive framework linking the casting process to the structural response. Simulations integrating casting and testing might contribute to further investigate the limitations and opportunities of the use of flowable FRC in load-carrying structures.

## ACKNOWLEDGMENTS

The authors wish to acknowledge support from COIN – the Concrete Innovation Centre ([www.coinweb.no](http://www.coinweb.no)) – a centre for research-based innovation, which was initiated by the Research Council of Norway (RCN) in 2006 for an eight-year period. The Centre was directed by SINTEF, with NTNU as a research partner, and the most recent industrial partners included Aker Solutions, Norcem, Norwegian Public Roads Administration, Rescon Mapei, Skanska, Unicon, Veidekke, and Weber Saint Gobain.

## REFERENCES

- Advani, S. G., & Tucker, C. L. (1987). The use of tensors to describe and predict fiber orientation in short fiber composites. *Journal of Rheology*, 31(8), 751-784. doi:10.1122/1.549945
- Barnett, S., Lataste, J.-F., Parry, T., Millard, S., & Soutsos, M. (2010). Assessment of fibre orientation in ultra high performance fibre reinforced concrete and its effect on flexural strength. *Materials and Structures*, 43(7), 1009-1023. doi:10.1617/s11527-009-9562-3
- Boulekbache, B., Hamrat, M., Chemrouk, M., & Amziane, S. (2010). Flowability of fibre-reinforced concrete and its effect on the mechanical properties of the material. *Construction and Building Materials*, 24(9), 1664-1671. doi:10.1016/j.conbuildmat.2010.02.025
- Chiachio, M., Chiachio, J., & Rus, G. (2012). Reliability in composites – A selective review and survey of current development. *Composites Part B: Engineering*, 43(3), 902-913. doi:10.1016/j.compositesb.2011.10.007
- Cunha, V. M. C. F., Barros, J. A. O., & Sena-Cruz, J. M. (2012). A finite element model with discrete embedded elements for fibre reinforced composites. *Computers & Structures*, 94–95(0), 22-33. doi:http://dx.doi.org/10.1016/j.compstruc.2011.12.005
- Døssland, Å. L. (2008). *Fibre Reinforcement in Load Carrying Concrete Structures*. (Doctoral thesis), Norwegian University of Science and Technology (NTNU), Trondheim. (2008:50)
- European Standard. (2005). Test method for metallic fibre concrete - Measuring the flexural tensile strength (limit of proportionality (LOP), residual). (Vol. EN 14651:2005+A1:2007). Brussels, Belgium: European Committee for Standardization.
- Ferrara, L., Bamonte, P., Caverzan, A., Musa, A., & Sanal, I. (2012). A comprehensive methodology to test the performance of Steel Fibre Reinforced Self-Compacting Concrete (SFR-SCC). *Construction and Building Materials*, 37, 406-424. doi:http://dx.doi.org/10.1016/j.conbuildmat.2012.07.057
- Ferrara, L., Ozyurt, N., & di Prisco, M. (2011). High mechanical performance of fibre reinforced cementitious composites: the role of “casting-flow induced” fibre orientation. *Materials and Structures*, 44(1), 109-128. doi:10.1617/s11527-010-9613-9
- fib. (2010). Model Code for Concrete Structures 2010, International Federation for Structural Concrete (fib).
- Grünewald, S., Laranjeira, F., Walraven, J. C., Aguado de Cea, A., & Molins Borrell, C. (2012). *Influence of fibre orientation on the performance of steel fibre-reinforced concrete*. Paper presented at the 8th RILEM International Symposium on Fiber Reinforced Concrete: challenges and opportunities (BEFIB 2012), Guimaraes, Portugal.
- Kooiman, A. G. (2000). *Modelling steel fibre reinforced concrete for structural design*. (Doctoral thesis), Delft University of Technology, Rotterdam, The Netherlands.
- Markovic, I. (2006). *High-Performance Hybrid-Fibre Concrete - Development and Utilization*. (Doctoral thesis), Delft University of Technology, Delft, The Netherlands.
- Rots, J. G. (1988). *Computational modeling of concrete fracture*. (Doctoral thesis), Delft University of Technology, Rotterdam, The Netherlands.
- Şanal, İ., & Özyurt Zihnioğlu, N. (2013). To what extent does the fiber orientation affect mechanical performance? *Construction and Building Materials*, 44(0), 671-681. doi:10.1016/j.conbuildmat.2013.03.079
- Sarmiento, E. V. (2015). *Flowable fibre-reinforced concrete for structural applications. A modelling approach that can take anisotropic and inhomogeneous fibre configuration into account*. (Doctoral thesis), Norwegian University of Science and Technology, Trondheim, Norway.

- Sarmiento, E. V., Hendriks, M. A. N., & Kanstad, T. (2014). Accounting for the fibre orientation on the structural performance of flowable fibre reinforced concrete. In N. Bićanić, H. Mang, G. Meschke, & R. de Borst (Eds.), *Computational Modelling of Concrete Structures* (Vol. 2, pp. 609-618): CRC Press.
- Soroushian, P., & Lee, C.-D. (1990). Distribution and orientation of fibres in steel fiber reinforced concrete. *Materials Journal*, *87*(5), 433-439. doi:10.14359/1803
- Stähli, P., Custer, R., & van Mier, J. G. M. (2008). On flow properties, fibre distribution, fibre orientation and flexural behaviour of FRC. *Materials and Structures*, *41*(1), 189-196. doi:10.1617/s11527-007-9229-x
- Stähli, P., & van Mier, J. G. M. (2007). Manufacturing, fibre anisotropy and fracture of hybrid fibre concrete. *Engineering Fracture Mechanics*, *74*(1-2), 223-242. doi:10.1016/j.engfracmech.2006.01.028
- Švec, O., & Skoček, J. (2013). Simple Navier's slip boundary condition for the non-Newtonian Lattice Boltzmann fluid dynamics solver. *Journal of Non-Newtonian Fluid Mechanics*, *199*, 61-69. doi:http://dx.doi.org/10.1016/j.jnnfm.2013.06.003
- Švec, O., Skoček, J., Stang, H., Geiker, M. R., & Roussel, N. (2012). Free surface flow of a suspension of rigid particles in a non-Newtonian fluid: A lattice Boltzmann approach. *Journal of Non-Newtonian Fluid Mechanics*, *179-180*, 32-42. doi:http://dx.doi.org/10.1016/j.jnnfm.2012.05.005
- Švec, O., Skoček, J., Stang, H., Olesen, J. F., & Poulsen, P. N. (2011). *Flow simulation of fiber reinforced self compacting concrete using Lattice Boltzmann method*. Paper presented at the 13th International Congress on the Chemistry of Cement (ICCC), Madrid, Spain.
- Švec, O., Žirgulis, G., Bolander, J. E., & Stang, H. (2014). Influence of formwork surface on the orientation of steel fibres within self-compacting concrete and on the mechanical properties of cast structural elements. *Cement and Concrete Composites*, *50*(0), 60-72. doi:10.1016/j.cemconcomp.2013.12.002
- Zhou, B., & Uchida, Y. (2013). *Fiber Orientation in Ultra High Performance Fiber Reinforced Concrete and its Visualization*. Paper presented at the Proceedings of the Eighth International Conference on Fracture Mechanics of Concrete and Concrete Structures, Toledo, Spain.
- Žirgulis, G., Švec, O., Geiker, M. R., Cwirzen, A., & Kanstad, T. (2016). Variation in fibre volume and orientation in walls: Experimental and numerical investigation. *Accepted for publication in Structural Concrete*.